

Analysis of Non-local Multicontinuum Upscaling for Dual Continuum Model

Jingyan Zhang* Siu Wun Cheung†

November 4, 2020

Abstract

In this paper, we develop and analyze a rigorous multiscale upscaling method for dual continuum model, which serves as a powerful tool in subsurface formation applications. Our proposed method is capable of identifying different continua and capturing non-local transfer and effective properties in the computational domain via constructing localized multiscale basis functions. The construction of the basis functions consists of solving local problems defined on oversampling computational region, subject to the energy minimizing constraints that the mean values of the local solution are zero in all continua except for the one targeted. The basis functions constructed are shown to have good approximation properties. It is shown that the method has a coarse mesh dependent convergence. We present some numerical examples to illustrate the performance of the proposed method.

1 Introduction

Subsurface formations exist in a variety of practical applications. In reservoir simulation, the material properties within fractures and background media can be significantly distinct. In the case of large fractures, Discrete Fracture Model (DFM) and Embedded Fracture Model (EFM) are used to explicitly define fracture networks with accuracy [28, 27, 22]. Explicitness for complex models is naturally in need of large system of equations, which will lead to large computational costs. Moreover, due to the multiple scales and high contrast properties intrinsic to the reservoir, performing high fidelity simulations for fractured porous media is a complex enough to cause extremely high computational costs.

To overcome this difficulty, research effort had been devoted to construct numerical solvers on a coarse grid, which is typically much coarser than the fine grid which captures all the heterogeneities in the medium properties. Typical approaches involve computing upscaled effective properties in each local coarse-grid block or representative volume [15, 37]. Such approaches are known to be insufficient when more than one important modes exist in the same coarse block or representative volume. In these cases, more efficient upscaling methods, typically the multicontinuum models, are employed [2, 3, 29, 32, 36, 38]. In such approaches, several effective properties are formulated in each coarse block and interaction terms are defined to characterize the transfer between different continua. Another class of methods are the multiscale methods, including Heterogeneous Multiscale Methods (HMM) [16, 1, 17], Variational Multiscale Methods (VMS) [24, 25, 26, 4] and Multiscale Finite Element Method (MsFEM) [23, 20]. Similar to upscaling approaches, multiscale scale is to construct numerical solvers on the coarse grid, which

*Department of Mathematics, Texas A&M University, College Station, TX 77843, USA (jingyanzhang@math.tamu.edu)

†Department of Mathematics, Texas A&M University, College Station, TX 77843, USA (tonycsw2905@math.tamu.edu)

is typically much coarser than the fine grid which captures all the heterogeneities in the medium properties. Instead of computing the effective medium properties, multiscale basis functions which are responsible for capturing the local oscillatory effects of the solution are constructed and coarse-scale macroscopic equations are formulated. The solution of the coarse-scale system can then be used to recover fine-scale information with the multiscale basis functions.

However, for more complex high-contrast heterogeneous media, each local coarse region contains several high-conductivity regions and multiple multiscale basis functions are required to represent the local solution space. The aforementioned multiscale methods typically use one basis function per coarse region, which is insufficient and may give rise to large error. To this end, it is crucial to systemically enrich the multiscale space with suitable fine-scale information for low-dimensional solution representation. One such approach is the Generalized Multiscale Finite Element Method (GMsFEM) [19, 18, 13, 8], which involves the construction appropriate snapshot space which consists of fine-scale data for solution representation by local snapshot problems and the construction of multiscale basis functions by performing feature extraction through local spectral decompositions to the snapshot space. Since multiscale basis functions are identified for multiscale solution representation in high-contrast heterogeneous media, multiple basis functions from the spectral problem are required to attain a small error. By introducing adaptivity [21, 8], one can add multiscale basis functions in selected regions. The connection of GMsFEM to multicontinuum models is discussed in [10], and GMsFEM are successfully applied to multicontinuum models that originate from fracture models and contain nonlinearities [35, 6, 31, 30].

More recently, a combination of GMsFEM and localization has been discussed in [11] as the approach of Constraint Energy Minimizing GMsFEM (CEM-GMsFEM). The method uses oversampling computational regions for the construction of multiscale basis functions. The first step is to find the auxiliary multiscale basis functions by GMsFEM. The second step is to construct multiscale basis functions by minimizing energy functionals subject to certain constraints, the purpose of which is to localize the multiscale basis functions. The method has been applied to various discretization and model problems [9, 7, 6, 5], and it has been theoretically and numerically verified that the multiscale solutions spanned by the multiscale basis functions in CEM-GMsFEM have both spectral convergence and mesh dependent convergence.

The construction of auxiliary multiscale functional space is key to identify high contrast channels and fractures in multicontinuum models. However, the adoption of GMsFEM in obtaining the auxiliary space is of relatively high computational cost. To modify the method, under the assumption that one knows the fracture network in each coarse-grid block, the method of nonlocal multicontinuum (NLMC) is proposed in [12, 39] and applied to fracture models [33, 34]. The aforementioned assumption is a main drawback to NLMC but is a scenario common in practice. Instead of solving local spectral problems GMsFEM, the auxiliary basis functions are defined to represent coarse-scale solution average in a straightforward manner. As is in CEM-GMsFEM, the multiscale basis functions are solved from problems formulated to minimize the local energy in an oversampling domain. The mass transfers between fractures and matrix is therefore non-local.

In this work, we develop and analyze the NLMC method for a dual continuum model. The auxiliary basis functions are simply defined in each coarse block for each continuum, which represents fractures and matrix. To be more precise, in each oversampling domain, the auxiliary basis functions are constant in a continuum, and each has mean value one for the chosen continuum and zero otherwise. Out of the oversampling domain, the value of the basis functions are zero. The degrees of freedom is the same as the number of the continua, which is the minimal number needed to represent the heterogeneous property of the reservoir. To obtain the multiscale basis functions, we solve local minimization problems in oversampling computational domain. We show that the minimizer has a good decay property. With a proper number of oversampling layers, the basis functions derived can well capture the fine-grid information. Moreover, we show that the method has a convergence dependent on coarse mesh size. We also present some

numerical examples to depict the performance of the method.

The paper is organized as follows. In Section 2 we present the dual continuum model. The proposed method is introduced in Section 3 and analyzed in Section 4. In Section 5 some numerical experiments are demonstrated to confirm the theory. The paper ends with conclusions in Section 6.

2 Dual continuum Model

We consider the following dual continuum model [3, 14, 36]

$$\begin{aligned} c_1 \frac{\partial p_1}{\partial t} - \operatorname{div}(\kappa_1 \nabla p_1) + \sigma(p_1 - p_2) &= f_1, \\ c_2 \frac{\partial p_2}{\partial t} - \operatorname{div}(\kappa_2 \nabla p_2) - \sigma(p_1 - p_2) &= f_2, \end{aligned} \tag{1}$$

in a computational domain $\Omega \subset \mathbb{R}^2$. Here, for $i = 1, 2$, c_i is the compressibility, p_i is the pressure, κ_i is the permeability, and f_i is the source function for the i -th continuum. In addition, the continua are coupled through the mass exchange, and σ is a parameter which accounts for the strength of mass transfer between the continua. One particular application of the dual continuum model (1) is to represent the global interactive effects of the unresolved fractures and the matrix. In this work, we consider high-contrast channelized media. We prescribe the initial condition $p_i(0, \cdot) = p_i^0$ in Ω and the boundary condition $p_i(t, \cdot) = 0$ on $\partial\Omega$ for $t > 0$.

Let $V = [H_0^1(\Omega)]^2$. Also, for a subdomain $D \subset \Omega$, we denote the restriction of V on D by $V(D)$. The weak formulation of (1) then reads: find $p = (p_1, p_2)$ such that $p(t, \cdot) \in V$ and

$$c \left(\frac{\partial p}{\partial t}, v \right) + a_Q(p, v) = (f, v), \tag{2}$$

for all $v = (v_1, v_2)$ with $v(t, \cdot) \in V$. Here, (\cdot, \cdot) denotes the standard $L^2(\Omega)$ inner product. Moreover, the bilinear forms are defined as:

$$\begin{aligned} c_i(p_i, v_i) &= \int_{\Omega} c_i(x) p_i v_i \, dx, \\ c(p, v) &= \sum_i c_i(p_i, v_i), \\ a_i(p_i, v_i) &= \int_{\Omega} \kappa_i(x) \nabla p_i \cdot \nabla v_i \, dx, \\ a(p, v) &= \sum_i a_i(p_i, v_i), \\ q(p, v) &= \sum_i \sum_{i'} \int_{\Omega} \sigma(p_i - p_{i'}) v_i \, dx, \\ a_Q(p, v) &= a(p, v) + q(p, v). \end{aligned} \tag{3}$$

3 Method description

In this section, we will describe our proposed method in detail. To start with, we introduce the concepts of coarse and fine meshes. We start with a plain partition of calculation domain Ω , \mathcal{T}^H . This partition is called a coarse mesh, which does not necessarily resolve any multiscale features. We denote one element in \mathcal{T}^H as K and name it as a coarse element. Here, $H > 0$ is the coarse mesh size. We denote the number of coarse elements and coarse grid nodes as N and N_c respectively. The collection of all coarse element edges is called \mathcal{E}^H . To sufficiently resolve

the solution, we refine the coarse mesh \mathcal{T}^H into a fine mesh \mathcal{T}^h , where $h > 0$ is called the fine mesh size. We remark that the fine grid system is only used in locally solving process, where all local problems are solved continuously. Therefore, we don't consider fine grid in our analysis hereinafter. A demonstration of coarse and fine meshes is given in Figure 1.

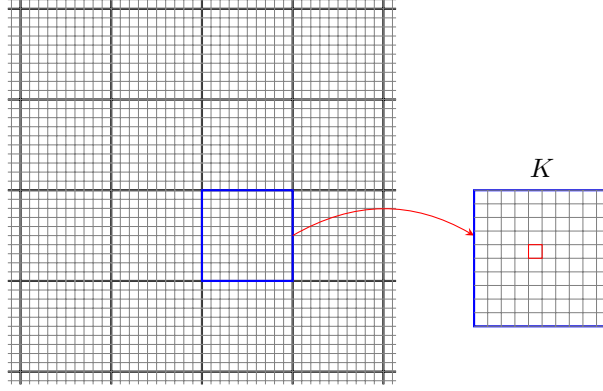


Figure 1: An illustration of the coarse and fine meshes.

Next, we clarify more notions concerning every coarse element. Letting $K_j \in \mathcal{T}^H$ be the j -th coarse element, an oversampling domain $K_{j,m}$ is defined by expanding K_j with m layers of coarse elements in Ω . An illustration is given in Figure 2. Moreover, similar to the partition of computational domain Ω , for $i = 1, 2$, we denote $K_j = \cup_{l=1}^{L_i^{(j)}} K_l^{(i,j)}$, where $L_i^{(j)}$ denotes the number of high conductive channels plus matrix within K_j for continua i .

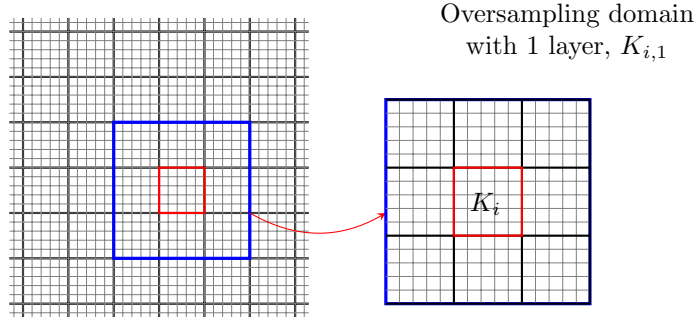


Figure 2: An illustration of oversampling domain.

We now proceed to describing the proposed method step by step.

Step 1. Definition of auxiliary basis functions. Within $K_j (j = 1, \dots, N)$, for each $l = 1, \dots, L_i^{(j)}$, we directly define our auxiliary basis function $\phi_l^{(i,j)} \in P^0(\mathcal{T}^h(K_{j,m}))$, where $\mathcal{T}^h(K_{j,m})$ denotes the restriction of \mathcal{T}^h on $K_{j,m}$, as

$$\phi_l^{(i,j)} = \frac{1}{|K_l^{(i,j)}|} \mathcal{I}_{K_l^{(i,j)}}. \quad (4)$$

Here, $|K_l^{(i,j)}|$ denotes the area of $K_l^{(i,j)}$ and $\mathcal{I}_{K_l^{(i,j)}}$ is the characteristic function. The local auxiliary space for continua i is constructed as

$$V_{\text{aux}}^{(i,j)} = \text{span}\{\phi_l^{(i,j)} | 1 \leq l \leq L_i^{(j)}\}. \quad (5)$$

Furthermore, we define the local auxiliary space as

$$V_{\text{aux}}^j = V_{\text{aux}}^{(1,j)} \times V_{\text{aux}}^{(2,j)}. \quad (6)$$

The global auxiliary space is defined as the direct sum of all local auxiliary spaces as

$$V_{\text{aux}} = \bigoplus_{j=1}^N V_{\text{aux}}^j. \quad (7)$$

Step 2. Construction of multiscale basis functions. For the convenience of describing the method and the subsequent convergence analysis, for all $v = (v_1, v_2) \in [L^2(K_j)]^2$, we introduce a local projection operator $\pi_j : [L^2(K_j)]^2 \rightarrow V_{\text{aux}}$ as

$$\pi_j(v) = \left(\sum_{l=1}^{L_1^{(j)}} (v_1, \phi_l^{(1,j)}) \phi_l^{(1,j)}, \sum_{l=1}^{L_2^{(j)}} (v_2, \phi_l^{(2,j)}) \phi_l^{(2,j)} \right) \quad (8)$$

and a global projection operator $\pi : [L^2(\Omega)]^2 \rightarrow V_{\text{aux}}$ is defined as

$$\pi(v) = \sum_{j=1}^N \pi_j(v), \quad \forall v \in [L^2(\Omega)]^2. \quad (9)$$

The local multiscale basis functions are constructed by the following variational form of minimization problem. Within the oversampling domain $K_{j,m}$ of every $K_j \subset \Omega$, find $\psi_{l,\text{ms}}^{(i,j)} \in V(K_{j,m})$ and $\bar{T}_{i',j',l'}^{i,j,l} \in \mathbb{R}$ such that for $i = 1, 2$, we have

$$\begin{aligned} a_Q(\psi_{l,\text{ms}}^{(i,j)}, w) + \sum_{i'=1}^2 \sum_{K_{l'}^{(i',j')} \subset K_{j,m}} \bar{T}_{i',j',l'}^{i,j,l} (w \cdot \mathbf{e}_{i'}, \phi_{l'}^{(i',j')}) &= 0, \quad \forall w \in V(K_{j,m}), \\ (\psi_{l,\text{ms}}^{(i,j)} \cdot \mathbf{e}_{i'}, \phi_{l'}^{(i',j')}) &= \delta_{i,i'} \delta_{l,l'} \delta_{j,j'}, \quad \forall K_{l'}^{(i',j')} \subset K_{j,m}. \end{aligned} \quad (10)$$

Here, \mathbf{e}_i is the canonical basis for \mathbb{R}^2 . $\delta_{i,i'}$, $\delta_{l,l'}$ and $\delta_{j,j'}$ are the delta Dirac function. We use the local multiscale basis functions to obtain the multiscale finite element space, which will be used for deriving the multiscale solution, as

$$V_{\text{ms}} = \text{span}\{\psi_{l,\text{ms}}^{(i,j)} | 1 \leq l \leq L_i^{(j)}, 1 \leq j \leq N, i = 1, 2\}. \quad (11)$$

The local multiscale basis functions are inspired from the global multiscale basis functions which are constructed in the similar way but on the global domain. For every coarse element K_j in Ω , find $\psi_l^{(i,j)} \in V$ and $T_{i',j',l'}^{i,j,l} \in \mathbb{R}$ such that

$$\begin{aligned} a_Q(\psi_l^{(i,j)}, w) + \sum_{i'=1}^2 \sum_{K_{l'}^{(i',j')} \subset \Omega} T_{i',j',l'}^{i,j,l} (w \cdot \mathbf{e}_{i'}, \phi_{l'}^{(i',j')}) &= 0, \quad \forall w \in V, \\ (\psi_l^{(i,j)} \cdot \mathbf{e}_{i'}, \phi_{l'}^{(i',j')}) &= \delta_{i,i'} \delta_{l,l'} \delta_{j,j'}, \quad \forall K_{l'}^{(i',j')} \subset \Omega. \end{aligned} \quad (12)$$

The global multiscale finite element space is thus defined as

$$V_{\text{glo}} = \text{span}\{\psi_l^{(i,j)} | 1 \leq l \leq L_i^{(j)}, 1 \leq j \leq N, i = 1, 2\}. \quad (13)$$

As our analysis suggest, the global basis functions exhibit exponential decay properties and have small values outside a sufficiently large oversampling region. The fact suggests that we can

save computational costs by localizing the basis functions by truncating the domain, without introducing huge error.

We remark that if we denote \tilde{V} as the null space of the global projection operator π , for any $\psi_l^{(i,j)} \in V_{\text{glo}}$, we have

$$a_Q(\psi_l^{(i,j)}, v) = 0, \quad \forall v \in \tilde{V}. \quad (14)$$

This implies that with respect to the inner product of a_Q , $\tilde{V} \subset V_{\text{glo}}^\perp$. As a matter of fact, $\tilde{V} = V_{\text{glo}}^\perp$.

Step 3. Multiscale solution. The process of finding the multiscale solution can be described as follows. Find $p_{\text{ms}} = (p_{\text{ms},1}, p_{\text{ms},2})$ with $p_{\text{ms}}(t, \cdot) \in V_{\text{ms}}$ s.t. for all $v = (v_1, v_2)$ with $v(t, \cdot) \in V_{\text{ms}}$,

$$c\left(\frac{\partial p_{\text{ms}}}{\partial t}, v\right) + a_Q(p_{\text{ms}}, v) = (f, v). \quad (15)$$

4 Convergence Analysis

In this section, we will analyze the proposed method. First, we define the following norms and semi-norms on V :

$$\begin{aligned} \|p\|_c^2 &= c(p, p), \\ \|p\|_a^2 &= a(p, p), \\ |p|_q^2 &= q(p, p), \\ \|p\|_{a_Q}^2 &= a_Q(p, p), \\ \|p\|_{\mathbb{L}^2(\Omega; \kappa)}^2 &= \sum_i (\kappa_i^{\frac{1}{2}} p_i, \kappa_i^{\frac{1}{2}} p_i), \\ \|p\|_{\mathbb{L}^2(\Omega; \kappa^{-1})}^2 &= \sum_i (\kappa_i^{-\frac{1}{2}} p_i, \kappa_i^{-\frac{1}{2}} p_i). \end{aligned} \quad (16)$$

For a subdomain $D = \bigcup_{j \in J} K_j$ as a union of coarse grid blocks, we also define the following local norms and semi-norms on V :

$$\begin{aligned} \|p\|_{a(D)}^2 &= \sum_{j \in J} a^{(j)}(p, p), \\ |p|_{q(D)}^2 &= \sum_{j \in J} q^{(j)}(p, p), \\ \|p\|_{a_Q(D)}^2 &= \sum_{j \in J} a_Q^{(j)}(p, p), \\ \|p\|_{\mathbb{L}^2(D; \kappa)}^2 &= \sum_{j \in J} (\kappa_i^{\frac{1}{2}} p_i, \kappa_i^{\frac{1}{2}} p_i)_{L^2(K_j)}, \\ \|p\|_{\mathbb{L}^2(D; \kappa^{-1})}^2 &= \sum_{j \in J} (\kappa_i^{-\frac{1}{2}} p_i, \kappa_i^{-\frac{1}{2}} p_i)_{L^2(K_j)}. \end{aligned} \quad (17)$$

We remark that

$$\begin{aligned} \|p\|_{\mathbb{L}^2(D; \kappa)} &\leq \bar{\kappa}^{\frac{1}{2}} \|p\|_{[L^2(D)]^2}, \\ \|p\|_{\mathbb{L}^2(D; \kappa^{-1})} &\leq \underline{\kappa}^{-\frac{1}{2}} \|p\|_{[L^2(D)]^2}. \end{aligned} \quad (18)$$

In addition, we introduce some operators which will be used in our analysis, namely $R_{\text{glo}} : V \rightarrow V_{\text{glo}}$ given by: for any $u \in V$, the image $R_{\text{glo}} u \in V_{\text{glo}}$ is defined by

$$a_Q(R_{\text{glo}} u, v) = a_Q(u, v), \quad \forall v \in V_{\text{glo}}, \quad (19)$$

and similarly, $R_{\text{ms}} : V \rightarrow V_{\text{ms}}$ given by: for any $u \in V$, the image $R_{\text{ms}}u \in V_{\text{ms}}$ is defined by

$$a_Q(R_{\text{ms}}u, v) = a_Q(u, v), \quad \forall v \in V_{\text{ms}}. \quad (20)$$

We also define $\mathcal{C} : V \rightarrow V$ given by: for any $u \in V$, the image $\mathcal{C}u \in V$ is defined by

$$(\mathcal{C}u, v) = c(u, v), \quad \forall v \in V. \quad (21)$$

Moreover, the operator $\mathcal{A} : D(\mathcal{A}) \rightarrow [L^2(\Omega)]^2$ is defined on a subspace $D(\mathcal{A}) \subset V$ by: for any $u \in D(\mathcal{A})$, the image $\mathcal{A}u \in [L^2(\Omega)]^2$ is defined by

$$(\mathcal{A}u, v) = a_Q(u, v), \quad \forall v \in V. \quad (22)$$

The following lemma shows that the projection operator R_{glo} has a good approximation property with respect to the a_Q -norm and L^2 -norm.

Lemma 1. *Let $u \in D(\mathcal{A})$, then we have $u - R_{\text{glo}}u \in \tilde{V}$ and*

$$\|u - R_{\text{glo}}u\|_{a_Q} \leq CH \|\mathcal{A}u\|_{\mathbb{L}^2(\Omega; \kappa^{-1})}. \quad (23)$$

and

$$\|u - R_{\text{glo}}u\|_{[L^2(\Omega)]^2} \leq CH^2 \underline{\kappa}^{-\frac{1}{2}} \|\mathcal{A}u\|_{\mathbb{L}^2(\Omega; \kappa^{-1})}. \quad (24)$$

Proof. By (19), we directly get $u - R_{\text{glo}}u \in V_{\text{glo}}$. This yields

$$a_Q(u - R_{\text{glo}}u, R_{\text{glo}}u) = 0. \quad (25)$$

Thus, we have

$$\begin{aligned} a_Q(u - R_{\text{glo}}u, u - R_{\text{glo}}u) &= a_Q(u - R_{\text{glo}}u, u) - a_Q(u - R_{\text{glo}}u, R_{\text{glo}}u) \\ &= a_Q(u - R_{\text{glo}}u, u) \\ &= a_Q(u, u - R_{\text{glo}}u) \\ &= (\mathcal{A}u, u - R_{\text{glo}}u) \\ &\leq \|\mathcal{A}u\|_{\mathbb{L}^2(\Omega; \kappa^{-1})} \|u - R_{\text{glo}}u\|_{\mathbb{L}^2(\Omega; \kappa)}. \end{aligned} \quad (26)$$

Since $u - R_{\text{glo}}u \in \tilde{V}$, we have $\pi_j(u - R_{\text{glo}}u) = 0$ for all $l = 1, 2, \dots, L_j$ and $j = 1, 2, \dots, N$. Moreover, the Poincaré inequality gives

$$\int_{K_l^{(i,j)}} [(u - R_{\text{glo}}u) \cdot \mathbf{e}_i]^2 \leq CH^2 \int_{K_l^{(i,j)}} |\nabla[(u - R_{\text{glo}}u) \cdot \mathbf{e}_i]|^2. \quad (27)$$

This yields that

$$\begin{aligned} \|(u - R_{\text{glo}}u)\|_{\mathbb{L}^2(\Omega; \kappa)}^2 &= \sum_i \left\| \kappa_i^{\frac{1}{2}} (u - R_{\text{glo}}u) \cdot \mathbf{e}_i \right\|_{L^2(\Omega)}^2 \\ &= \sum_i \sum_{K_l^{(i,j)} \subset \Omega} \left\| \kappa_i^{\frac{1}{2}} (u - R_{\text{glo}}u) \cdot \mathbf{e}_i \right\|_{L^2(K_l^{(i,j)})}^2 \\ &\leq CH^2 \|u - R_{\text{glo}}u\|_{a_Q}^2. \end{aligned} \quad (28)$$

Thus, we have

$$\|u - R_{\text{glo}}u\|_{a_Q}^2 \leq CH \|\mathcal{A}u\|_{\mathbb{L}^2(\Omega; \kappa^{-1})} \|u - R_{\text{glo}}u\|_{a_Q}, \quad (29)$$

which gives the estimate in the (23).

The proof of (24) follows a duality argument. Define $w \in V$ such that

$$a_Q(w, v) = (u - R_{\text{glo}}u, v) \quad \forall v \in V. \quad (30)$$

Then we have

$$\|u - R_{\text{glo}}u\|_{[L^2(\Omega)]^2}^2 = (u - R_{\text{glo}}u, u - R_{\text{glo}}u) = a_Q(w, u - R_{\text{glo}}u). \quad (31)$$

Taking $v = R_{\text{glo}}w \in V_{\text{glo}}$ in (19), we obtain

$$a_Q(u - R_{\text{glo}}u, R_{\text{glo}}w) = 0. \quad (32)$$

Since $w \in D(\mathcal{A})$ and $\mathcal{A}w = u - R_{\text{glo}}u$, we have

$$\begin{aligned} \|u - R_{\text{glo}}u\|_{[L^2(\Omega)]^2}^2 &= a_Q(w - R_{\text{glo}}w, u - R_{\text{glo}}u) \\ &\leq \|w - R_{\text{glo}}w\|_{a_Q} \|u - R_{\text{glo}}u\|_{a_Q} \\ &\leq \left(CH \|\mathcal{A}w\|_{\mathbb{L}^2(\Omega; \kappa^{-1})} \right) \left(CH \|\mathcal{A}u\|_{\mathbb{L}^2(\Omega; \kappa^{-1})} \right) \\ &\leq \left(CH \underline{\kappa}^{-\frac{1}{2}} \|\mathcal{A}w\|_{[L^2(\Omega)]^2} \right) \left(CH \|\mathcal{A}u\|_{\mathbb{L}^2(\Omega; \kappa^{-1})} \right) \\ &\leq CH^2 \underline{\kappa}^{-\frac{1}{2}} \|u - R_{\text{glo}}u\|_{[L^2(\Omega)]^2} \|\mathcal{A}u\|_{\mathbb{L}^2(\Omega; \kappa^{-1})}. \end{aligned} \quad (33)$$

□

Next, we show that the global basis functions are localizable. For the purpose of this, for each coarse block K , we define a bubble function B such that $B(x) > 0, \forall x \in \text{int}(K)$ and $B(x) = 0, \forall x \in \partial K$. We will take $B = \prod_{x_k} \chi_k^H$, where χ_k^H is coarse scale partition of unity on K . Based on the bubble function, we define a constant as follows.

$$C_{\text{equiv}} = \sup_{K_j \in \mathcal{T}^H, v \in V_{\text{aux}}} \frac{\|v\|_{[L^2(K_j)]^2}^2}{\left\| B^{\frac{1}{2}} v \right\|_{[L^2(K_j)]^2}^2}. \quad (34)$$

Lemma 2. *For all $v_{\text{aux}} \in V_{\text{aux}}$, there exists a function $v \in V$ such that*

$$\pi(v) = v_{\text{aux}}, \quad \|v\|_{a_Q}^2 \leq D \|v_{\text{aux}}\|_{\mathbb{L}^2(\Omega; \kappa)}^2, \quad \text{supp}(v) \subset \text{supp}(v_{\text{aux}}), \quad (35)$$

where $D = \frac{C_{\mathcal{T}}^2}{H^2} + 2 \max_i \left\| \frac{\sigma_i}{\kappa_i} \right\|_{L^\infty(\Omega)}$ and $C_{\mathcal{T}}$ is the maximum of vertices over all coarse elements.

Proof. Without loss of generality we assume $v_{\text{aux}} \in V_{\text{aux}}^j$ with $\|v_{\text{aux}}\|_{[L^2(K_j)]^2} = 1$. We consider the following saddle point problem: find $v \in V_0(K_j)$ and $T_{l'}^{i'} \in \mathbb{R}$ such that

$$\begin{aligned} a_Q(v, w) + \sum_{i'=1}^2 \sum_{K_l^{(i',j)} \subset K_j} T_{l'}^{i'} (w \cdot \mathbf{e}_{i'}, \phi_{l'}^{(i',j)}) &= 0, \quad \forall w \in V_0(K_j), \\ ((v - v_{\text{aux}}) \cdot \mathbf{e}_{i'}, \phi_{l'}^{(i',j)}) &= 0, \quad \forall K_l^{(i',j)} \subset K_j. \end{aligned} \quad (36)$$

The well-posedness of the above saddle point problem is equivalent to the existence of $\tilde{v} \in V_0(K_j)$ such that

$$(\tilde{v}, v_{\text{aux}}) \geq C_1 \|v_{\text{aux}}\|_{\mathbb{L}^2(K_j; \kappa)}^2, \quad \|\tilde{v}\|_{a_Q(K_j)} \leq C_2 \|v_{\text{aux}}\|_{\mathbb{L}^2(K_j; \kappa)}, \quad (37)$$

where C_1, C_2 are constants to be determined. Taking $\tilde{v} = Bv_{\text{aux}}$, we have

$$(\tilde{v}, v_{\text{aux}}) = \left\| B^{\frac{1}{2}} v_{\text{aux}} \right\|_{[L^2(K_j)]^2}^2 \geq C_{\text{equiv}}^{-1} \|v_{\text{aux}}\|_{[L^2(K_j)]^2}^2. \quad (38)$$

On the other hand, on every $K_l^{(i,j)}$, we have

$$\nabla(\tilde{v} \cdot \mathbf{e}_i) = B\nabla(\tilde{v} \cdot \mathbf{e}_i) + \nabla B(\tilde{v} \cdot \mathbf{e}_i). \quad (39)$$

By definition of V_{aux} , $\|B\nabla(\tilde{v} \cdot \mathbf{e}_i)\|_{L^2(K_j)} = 0$. At the same time, $|B| \leq 1$, $|\nabla B| \leq C_{\mathcal{T}}H^{-1}$. Thus,

$$\left\| \kappa_i^{\frac{1}{2}} \nabla(\tilde{v} \cdot \mathbf{e}_i) \right\|_{L^2(K_j)}^2 \leq \frac{C_{\mathcal{T}}^2}{H^2} \|\kappa_i(\tilde{v} \cdot \mathbf{e}_i)\|_{L^2(K_j)}^2. \quad (40)$$

This yields

$$\|\tilde{v}\|_{a(K_j)}^2 \leq \frac{C_{\mathcal{T}}^2}{H^2} \sum_i \left\| \kappa_i^{\frac{1}{2}} (v_{\text{aux}} \cdot \mathbf{e}_i) \right\|_{L^2(K_j)}^2 \quad (41)$$

and

$$|\tilde{v}|_{q(K_j)}^2 \leq 2 \max_i \left\| \frac{\sigma_i}{\kappa_i} \right\|_{L^\infty(K_j)} \sum_i \left\| \kappa_i^{\frac{1}{2}} (v_{\text{aux}} \cdot \mathbf{e}_i) \right\|_{L^2(K_j)}^2. \quad (42)$$

Thus, we have

$$\|\tilde{v}\|_{a_Q(K_j)}^2 \leq \left(\frac{C_{\mathcal{T}}^2}{H^2} + 2 \max_i \left\| \frac{\sigma_i}{\kappa_i} \right\|_{L^\infty(\Omega)} \right) \|v_{\text{aux}}\|_{\mathbb{L}^2(K_j; \kappa)}^2, \quad (43)$$

This guarantees the existence and uniqueness of $v \in V_0(K_j)$ and $T_{\nu'}^{i'} \in \mathbb{R}$ satisfying (36), in which v satisfies our desired properties. \square

Here, we make a remark that we can assume $D \geq 1$ without loss of generality.

In order to estimate the difference between the global basis functions and localized basis functions, we need the notion of a cutoff function with respect to the oversampling regions. For each coarse grid K_j and $M > m$, we define $\chi_j^{M,m} \in \text{span}\{\chi_k^H\}$ such that $0 \leq \chi_j^{M,m} \leq 1$ and $\chi_j^{M,m} = 1$ on the inner region $K_{j,m}$ and $\chi_j^{M,m} = 0$ outside the region $K_{j,M}$.

The following lemma shows that our multiscale basis functions have a decay property. In particular, the global basis functions are small outside an oversampling region specified in the lemma, which is important in localizing the multiscale basis functions.

Lemma 3. *Given $\phi_l^{(i,j)} \in V_{\text{aux}}^j$ and an oversampling region $K_{j,m}$ with number of layers $m \geq 2$. Let $\psi_{l,ms}^{(i,j)}$ be a localized multiscale basis function defined on $K_{j,m}$ given by (10), and $\psi_l^{(i,j)}$ be the corresponding global basis function given by (12). Then we have*

$$\left\| \psi_l^{(i,j)} - \psi_{l,ms}^{(i,j)} \right\|_{a_Q}^2 \leq E \left\| \phi_l^{(i,j)} \right\|_{\mathbb{L}^2(K_j; \kappa)}^2, \quad (44)$$

where $E = 8D(2+D)(1+CH^2) \left(1 + (C^{\frac{1}{2}}D^{\frac{1}{2}}H + CH^2)^{-1} \right)^{1-m}$.

Proof. By Lemma 2, there exists $v \in V$ such that

$$\pi(v) = \phi_l^{(i,j)}, \quad \|v\|_{a_Q}^2 \leq D \left\| \phi_l^{(i,j)} \right\|_{\mathbb{L}^2(\Omega; \kappa)}^2, \quad \text{supp}(v) \subset K_j. \quad (45)$$

We take $\eta = \psi_l^{(i,j)} - v \in V$ and $\zeta = v - \psi_{l,ms}^{(i,j)} \in V(K_{j,m})$. Then $\pi(\eta) = \pi(\zeta) = 0$ and hence $\eta, \zeta \in \tilde{V}$. We first see that for $K_{j'} \subset K_{j,m-1}$,

$$\pi_{j'}(\chi_j^{m,m-1}\eta) = \pi_{j'}(\eta) = 0, \quad (46)$$

since $\chi_j^{m,m-1} = 1$ on $K_{j,m-1}$ and $\eta \in \tilde{V}$. On the other hand, for $K_{j'} \subset \Omega \setminus K_{j,m}$,

$$\pi_{j'}(\chi_j^{m,m-1}\eta) = \pi_{j'}(0) = 0, \quad (47)$$

since $\chi_j^{m,m-1} = 0$ on $\Omega \setminus K_{j,m}$. Therefore, we have $\text{supp}(\pi(\chi_j^{m,m-1}\eta)) \subset K_{j,m} \setminus K_{j,m-1}$. Again, by Lemma 2, there exists $\beta \in V$ such that

$$\pi(\beta) = \pi(\chi_j^{m,m-1}\eta), \quad \|\beta\|_{a_Q}^2 \leq D \left\| \pi(\chi_j^{m,m-1}\eta) \right\|_{\mathbb{L}^2(K_{j,m} \setminus K_{j,m-1}; \kappa)}^2, \quad \text{supp}(\beta) \subset K_{j,m} \setminus K_{j,m-1}. \quad (48)$$

Take $\tau = \beta - \chi_j^{m,m-1}\eta \in V(K_{j,m})$. Again, $\pi(\tau) = 0$ and hence $\tau \in \tilde{V}$. Now, by the variational problems (12) and (10), we have

$$\begin{aligned} a_Q(\psi_l^{(i,j)}, w) + \sum_{i'=1}^2 \sum_{K_{l'}^{(i',j')} \subset \Omega} T_{i',j',l'}^{i,j,l}(w \cdot \mathbf{e}_{i'}, \phi_{l'}^{(i',j')}) &= 0, \quad \forall w \in V, \\ a_Q(\psi_{l,\text{ms}}^{(i,j)}, w) + \sum_{i'=1}^2 \sum_{K_{l'}^{(i',j')} \subset K_{j,m}} \bar{T}_{i',j',l'}^{i,j,l}(w \cdot \mathbf{e}_{i'}, \phi_{l'}^{(i',j')}) &= 0, \quad \forall w \in V(K_{j,m}) \end{aligned} \quad (49)$$

Taking $w = \tau - \zeta \in V(K_{j,m})$ and using the fact that $\tau - \zeta \in \tilde{V}$, we have

$$a_Q(\psi_l^{(i,j)} - \psi_{l,\text{ms}}^{(i,j)}, \tau - \zeta) = 0, \quad (50)$$

which implies

$$\begin{aligned} \left\| \psi_l^{(i,j)} - \psi_{l,\text{ms}}^{(i,j)} \right\|_{a_Q}^2 &= a_Q(\psi_l^{(i,j)} - \psi_{l,\text{ms}}^{(i,j)}, \psi_l^{(i,j)} - \psi_{l,\text{ms}}^{(i,j)}) \\ &= a_Q(\psi_l^{(i,j)} - \psi_{l,\text{ms}}^{(i,j)}, \eta + \zeta) \\ &= a_Q(\psi_l^{(i,j)} - \psi_{l,\text{ms}}^{(i,j)}, \eta + \tau) \\ &\leq \left\| \psi_l^{(i,j)} - \psi_{l,\text{ms}}^{(i,j)} \right\|_{a_Q} \|\eta + \tau\|_{a_Q}. \end{aligned} \quad (51)$$

By (48), we have

$$\begin{aligned} \left\| \psi_l^{(i,j)} - \psi_{l,\text{ms}}^{(i,j)} \right\|_{a_Q}^2 &\leq \|\eta + \tau\|_{a_Q}^2 \\ &= \left\| (1 - \chi_j^{m,m-1})\eta + \beta \right\|_{a_Q}^2 \\ &\leq 2 \left(\left\| (1 - \chi_j^{m,m-1})\eta \right\|_{a_Q}^2 + \|\beta\|_{a_Q}^2 \right) \\ &\leq 2 \left(\left\| (1 - \chi_j^{m,m-1})\eta \right\|_{a_Q}^2 + D \left\| \chi_j^{m,m-1}\eta \right\|_{\mathbb{L}^2(K_{j,m} \setminus K_{j,m-1}; \kappa)}^2 \right). \end{aligned} \quad (52)$$

For the first term on the right hand side of (52), since

$$\nabla \left((1 - \chi_j^{m,m-1})(\eta \cdot \mathbf{e}_i) \right) = (1 - \chi_j^{m,m-1})\nabla(\eta \cdot \mathbf{e}_i) - (\eta \cdot \mathbf{e}_i)\nabla\chi_j^{m,m-1}, \quad (53)$$

and $|1 - \chi_j^{m,m-1}| \leq 1$, we have

$$\left\| (1 - \chi_j^{m,m-1})\eta \right\|_a^2 \leq 2 \left(\|\eta\|_{a(\Omega \setminus K_{j,m-1})}^2 + \|\eta\|_{\mathbb{L}^2(\Omega \setminus K_{j,m-1}; \kappa)}^2 \right). \quad (54)$$

On the other hand, we have

$$|(1 - \chi_j^{m,m-1})\eta|_q^2 \leq |\eta|_q^2(\Omega \setminus K_{j,m-1}). \quad (55)$$

Therefore, we arrive at

$$\left\| (1 - \chi_j^{m,m-1})\eta \right\|_{a_Q}^2 \leq 2 \left(\|\eta\|_{a_Q(\Omega \setminus K_{j,m-1})}^2 + \|\eta\|_{\mathbb{L}^2(\Omega \setminus K_{j,m-1}; \kappa)}^2 \right). \quad (56)$$

For the second term on the right hand side of (52), using the fact that $|\chi_j^{m,m-1}| \leq 1$, we have

$$\begin{aligned} \left\| \pi(\chi_j^{m,m-1}\eta) \right\|_{\mathbb{L}^2(K_{j,m} \setminus K_{j,m-1}; \kappa)}^2 &\leq \left\| \chi_j^{m,m-1}\eta \right\|_{\mathbb{L}^2(K_{j,m} \setminus K_{j,m-1}; \kappa)}^2 \\ &\leq \|\eta\|_{\mathbb{L}^2(K_{j,m} \setminus K_{j,m-1}; \kappa)}^2. \end{aligned} \quad (57)$$

To sum up, we have

$$\left\| \psi_l^{(i,j)} - \psi_{l,\text{ms}}^{(i,j)} \right\|_{a_Q}^2 \leq 4 \|\eta\|_{a_Q(\Omega \setminus K_{j,m-1})}^2 + (4 + 2D) \|\eta\|_{\mathbb{L}^2(\Omega \setminus K_{j,m-1}; \kappa)}^2. \quad (58)$$

Since $\eta \in \tilde{V}$, using Poincaré inequality, we obtain

$$\|\eta\|_{\mathbb{L}^2(\Omega \setminus K_{j,m-1}; \kappa)}^2 \leq CH^2 \|\eta\|_{a_Q(\Omega \setminus K_{j,m-1})}^2. \quad (59)$$

Combining all the estimates, we have

$$\left\| \psi_l^{(i,j)} - \psi_{l,\text{ms}}^{(i,j)} \right\|_{a_Q}^2 \leq (4 + 2D)(1 + CH^2) \|\eta\|_{a_Q(\Omega \setminus K_{j,m-1})}^2. \quad (60)$$

Next, we will prove a recursive estimate for $\|\eta\|_{a_Q(\Omega \setminus K_{j,m-1})}^2$. We take $\xi = 1 - \chi_j^{m-1, m-2}$. Then $\xi = 1$ in $\Omega \setminus K_{j,m-1}$ and $0 \leq \xi \leq 1$. Hence, using

$$\nabla(\xi^2(\eta \cdot \mathbf{e}_i)) = \xi^2 \nabla(\eta \cdot \mathbf{e}_i) + 2\xi(\eta \cdot \mathbf{e}_i) \nabla \xi, \quad (61)$$

we have

$$|\xi \eta|_a^2 = a(\eta, \xi^2 \eta) + \|\eta\|_{\mathbb{L}^2(K_{j,m-1} \setminus K_{j,m-2}; \kappa)}^2, \quad (62)$$

which results in

$$\|\eta\|_{a_Q(\Omega \setminus K_{j,m-1})}^2 \leq \|\xi \eta\|_{a_Q}^2 \leq a_Q(\eta, \xi^2 \eta) + \|\eta\|_{\mathbb{L}^2(K_{j,m-1} \setminus K_{j,m-2}; \kappa)}^2. \quad (63)$$

We will estimate the first term on the right hand side of (63). Following the preceding argument, we see that $\text{supp}(\pi(\xi^2 \eta)) \subset K_{j,m-1} \setminus K_{j,m-2}$. By Lemma 2, there exists $\gamma \in V$ such that

$$\pi(\gamma) = \pi(\xi^2 \eta), \quad \|\gamma\|_{a_Q}^2 \leq D \|\pi(\xi^2 \eta)\|_{\mathbb{L}^2(K_{j,m-1} \setminus K_{j,m-2}; \kappa)}^2, \quad \text{supp}(\gamma) \subset K_{j,m-1} \setminus K_{j,m-2}. \quad (64)$$

Take $\theta = \xi^2 \eta - \gamma$. Again, $\pi(\theta) = 0$ and hence $\theta \in \tilde{V}$. Therefore, we have

$$a_Q(\psi_l^{(i,j)}, \theta) = 0. \quad (65)$$

Additionally, $\text{supp}(\theta) \subset \Omega \setminus K_{j,m-2}$. Recall that, in (45), we have $\text{supp}(v) \subset K_j$. Hence θ and v have disjoint supports, and

$$a_Q(v, \theta) = 0. \quad (66)$$

Therefore, we obtain

$$a_Q(\eta, \theta) = a_Q(\psi_l^{(i,j)}, \theta) - a_Q(v, \theta) = 0. \quad (67)$$

Note that $\xi^2 \eta = \theta + \gamma$. Using (64), we have

$$\begin{aligned} a_Q(\eta, \xi^2 \eta) &= a_Q(\eta, \gamma) \\ &\leq \|\eta\|_{a_Q(K_{j,m-1} \setminus K_{j,m-2})} \|\gamma\|_{a_Q(K_{j,m-1} \setminus K_{j,m-2})} \\ &\leq D^{\frac{1}{2}} \|\eta\|_{a_Q(K_{j,m-1} \setminus K_{j,m-2})} \|\pi(\xi^2 \eta)\|_{\mathbb{L}^2(K_{j,m-1} \setminus K_{j,m-2}; \kappa)}. \end{aligned} \quad (68)$$

Since $|\xi| \leq 1$, we have

$$\|\pi(\xi^2 \eta)\|_{\mathbb{L}^2(K_{j,m-1} \setminus K_{j,m-2}; \kappa)} \leq \|\xi^2 \eta\|_{\mathbb{L}^2(K_{j,m-1} \setminus K_{j,m-2}; \kappa)} \leq \|\eta\|_{\mathbb{L}^2(K_{j,m-1} \setminus K_{j,m-2}; \kappa)}. \quad (69)$$

Hence, the right hand side of (63) can be estimated by

$$\|\eta\|_{a_Q(\Omega \setminus K_{j,m-1})}^2 \leq D^{\frac{1}{2}} \|\eta\|_{a_Q(K_{j,m-1} \setminus K_{j,m-2})} \|\eta\|_{\mathbb{L}^2(K_{j,m-1} \setminus K_{j,m-2}; \kappa)} + \|\eta\|_{\mathbb{L}^2(K_{j,m-1} \setminus K_{j,m-2}; \kappa)}^2. \quad (70)$$

Since $\pi(\eta) = 0$, using Poincaré inequality, we have

$$\|\eta\|_{\mathbb{L}^2(K_{j,m-1} \setminus K_{j,m-2}; \kappa)} \leq CH^2 \|\eta\|_{a_Q(K_{j,m-1} \setminus K_{j,m-2})}^2, \quad (71)$$

which implies

$$\|\eta\|_{a_Q(\Omega \setminus K_{j,m-1})}^2 \leq (C^{\frac{1}{2}} D^{\frac{1}{2}} H + CH^2) \|\eta\|_{a_Q(K_{j,m-1} \setminus K_{j,m-2})}^2. \quad (72)$$

Therefore,

$$\begin{aligned} \|\eta\|_{a_Q(\Omega \setminus K_{j,m-2})}^2 &= \|\eta\|_{a_Q(\Omega \setminus K_{j,m-1})}^2 + \|\eta\|_{a_Q(K_{j,m-1} \setminus K_{j,m-2})}^2 \\ &\geq \left(1 + (C^{\frac{1}{2}} D^{\frac{1}{2}} H + CH^2)^{-1}\right) \|\eta\|_{a_Q(\Omega \setminus K_{j,m-1})}^2. \end{aligned} \quad (73)$$

Inductively, we have

$$\begin{aligned} \|\eta\|_{a_Q(\Omega \setminus K_{j,m-1})}^2 &\leq \left(1 + (C^{\frac{1}{2}} D^{\frac{1}{2}} H + CH^2)^{-1}\right)^{1-m} \|\eta\|_{a_Q(\Omega \setminus K_j)}^2 \\ &\leq \left(1 + (C^{\frac{1}{2}} D^{\frac{1}{2}} H + CH^2)^{-1}\right)^{1-m} \|\eta\|_{a_Q}^2. \end{aligned} \quad (74)$$

Finally, we estimate the term on the right hand side of (74). Recall from the first property of v in (45), we have $\pi(v) = \phi_l^{(i,j)}$, which implies

$$(v \cdot \mathbf{e}_{i'}, \phi_{i'}^{(i',j')}) = \delta_{i,i'} \delta_{l,l'} \delta_{j,j'}, \quad \forall K_{i'}^{(i',j')} \subset \Omega. \quad (75)$$

Taking $w = \eta$ in (12), we have

$$a_Q(\psi_l^{(i,j)}, \eta) = 0, \quad (76)$$

which implies

$$\|\psi_l^{(i,j)}\|_{a_Q} \leq \|v\|_{a_Q}. \quad (77)$$

Using a triangle inequality and the second property of v in (45), we have

$$\|\eta\|_{a_Q} = \left\| \psi_l^{(i,j)} - v \right\|_{a_Q} \leq 2 \|v\|_{a_Q} \leq 2D^{\frac{1}{2}} \left\| \phi_l^{(i,j)} \right\|_{\mathbb{L}^2(K_j; \kappa)}. \quad (78)$$

Combining (60), (74) and (78), we obtain our desired result. \square

The following lemma shows that, similar to the global projection operator R_{glo} , our localized multiscale finite element projection operator R_{ms} can also provide a good approximation with respect to the a_Q -norm and L^2 -norm.

Lemma 4. *Let $u \in D(\mathcal{A})$. Let $m \geq 2$ be the number of coarse grid layers in the oversampling regions in (10). If $m = O(\log(\frac{\bar{\kappa}}{H}))$, we have*

$$\|u - R_{\text{ms}}u\|_{a_Q} \leq CH \|\mathcal{A}u\|_{\mathbb{L}^2(\Omega; \kappa^{-1})}. \quad (79)$$

and

$$\|u - R_{\text{ms}}u\|_{[L^2(\Omega)]^2} \leq CH^2 \bar{\kappa}^{-\frac{1}{2}} \|\mathcal{A}u\|_{\mathbb{L}^2(\Omega; \kappa^{-1})}. \quad (80)$$

Proof. We write

$$R_{\text{glo}}u = \sum_{i=1}^2 \sum_{j=1}^N \sum_{l=1}^{L_i^{(j)}} \alpha_l^{(i,j)} \psi_l^{(i,j)} \in V_{\text{glo}} \quad (81)$$

and define

$$w = \sum_{i=1}^2 \sum_{j=1}^N \sum_{l=1}^{L_i^{(j)}} \alpha_l^{(i,j)} \psi_{l,\text{ms}}^{(i,j)} \in V_{\text{ms}}. \quad (82)$$

By (20), we have

$$\|u - R_{\text{ms}}u\|_{a_Q} \leq \|u - w\|_{a_Q} \leq \|u - R_{\text{glo}}u\|_{a_Q} + \|R_{\text{glo}}u - w\|_{a_Q} \quad (83)$$

By Lemma 3, we have that

$$\begin{aligned} \|R_{\text{glo}}u - w\|_{a_Q}^2 &= \left\| \sum_{i=1}^2 \sum_{j=1}^N \sum_{l=1}^{L_i^{(j)}} \alpha_l^{(i,j)} (\psi_l^{(i,j)} - \psi_{l,\text{ms}}^{(i,j)}) \right\|_{a_Q}^2 \\ &\leq C(m+1)^2 \sum_{j=1}^N \left\| \sum_{i=1}^2 \sum_{l=1}^{L_i^{(j)}} \alpha_l^{(i,j)} (\psi_l^{(i,j)} - \psi_{l,\text{ms}}^{(i,j)}) \right\|_{a_Q}^2 \\ &\leq CE(m+1)^2 \sum_{j=1}^N \left\| \sum_{i=1}^2 \sum_{l=1}^{L_i^{(j)}} \alpha_l^{(i,j)} \phi_l^{(i,j)} \right\|_{\mathbb{L}^2(K_j;\kappa)}^2 \\ &\leq CE(m+1)^2 \|R_{\text{glo}}u\|_{\mathbb{L}^2(\Omega;\kappa)}^2. \end{aligned} \quad (84)$$

Combining (83), (84) and Lemma 1, we have

$$\|u - R_{\text{ms}}u\|_{a_Q} \leq CH \|\mathcal{A}u\|_{\mathbb{L}^2(\Omega;\kappa^{-1})} + CE^{\frac{1}{2}}(m+1) \|R_{\text{glo}}u\|_{\mathbb{L}^2(\Omega;\kappa)}. \quad (85)$$

Now, we estimate $\|R_{\text{glo}}u\|_{\mathbb{L}^2(\Omega;\kappa)}^2$. By Poncaré inequality, we have

$$\|R_{\text{glo}}u\|_{\mathbb{L}^2(\Omega;\kappa)}^2 \leq \bar{\kappa} \|R_{\text{glo}}u\|_{[L^2(\Omega)]^2}^2 \leq C_p \bar{\kappa} \underline{\kappa}^{-1} \|R_{\text{glo}}u\|_{a_Q}^2. \quad (86)$$

Taking $v = R_{\text{glo}}u$ in (19) and by Cauchy-Schwarz inequality, we obtain

$$\|R_{\text{glo}}u\|_{a_Q}^2 = a_Q(u, R_{\text{glo}}u) = (\mathcal{A}u, R_{\text{glo}}u) \leq \|\mathcal{A}u\|_{\mathbb{L}^2(\Omega;\kappa^{-1})} \|R_{\text{glo}}u\|_{\mathbb{L}^2(\Omega;\kappa)}. \quad (87)$$

Combining (86) and (87), we obtain

$$\|R_{\text{glo}}u\|_{\mathbb{L}^2(\Omega;\kappa)} \leq C \bar{\kappa} \underline{\kappa}^{-1} \|\mathcal{A}u\|_{\mathbb{L}^2(\Omega;\kappa^{-1})}. \quad (88)$$

This yields

$$\|u - R_{\text{ms}}u\|_{a_Q} \leq C(H + \bar{\kappa} \underline{\kappa}^{-1} E^{\frac{1}{2}}(m+1)) \|\mathcal{A}u\|_{\mathbb{L}^2(\Omega;\kappa^{-1})} \quad (89)$$

To obtain desired result, we will need

$$H^{-1} \bar{\kappa} \underline{\kappa}^{-1} E^{\frac{1}{2}}(m+1) = O(1). \quad (90)$$

Taking logarithm, we have

$$\log(H^{-1}) + \log(\bar{\kappa}) - \log(\underline{\kappa}) + \frac{1-m}{2} \log\left(1 + (C^{\frac{1}{2}} D^{\frac{1}{2}} H + CH^2)^{-1}\right) = O(1). \quad (91)$$

Therefore, if we take $m = O\left(\log\left(\frac{\bar{\kappa}}{H}\right)\right)$, we have (79). The proof of (80) follows a similar duality argument as in Lemma 1. \square

Now we are ready to obtain our main theorem on estimating error between p and p_{ms} .

Theorem 5. *Suppose $f \in [L^2(\Omega)]^2$. Let $m \geq 2$ be the number of coarse grid layers of the oversampling domain in (10). Let p be the solution of (2) and p_{ms} of (15). If $m = O(\log(\frac{\kappa}{H}))$, we have*

$$\|p(T, \cdot) - p_{\text{ms}}(T, \cdot)\|_c^2 + \int_0^T \|p - p_{\text{ms}}\|_{a_Q}^2 dt \leq CH^2 \underline{\kappa}^{-1} \left(\|p^0\|_{a_Q}^2 + \int_0^T \|f\|_{[L^2(\Omega)]^2}^2 dt \right). \quad (92)$$

Proof. Taking $v = \frac{\partial p}{\partial t}$ in (2), we have

$$\left\| \frac{\partial p}{\partial t} \right\|_c^2 + \frac{1}{2} \frac{d}{dt} \|p\|_{a_Q}^2 = \left(f, \frac{\partial p}{\partial t} \right) \leq C \|f\|_{[L^2(\Omega)]^2}^2 + \frac{1}{2} \left\| \frac{\partial p}{\partial t} \right\|_c^2. \quad (93)$$

Integrating over $(0, T)$, we have

$$\frac{1}{2} \int_0^T \left\| \frac{\partial p}{\partial t} \right\|_c^2 dt + \frac{1}{2} \|p(T, \cdot)\|_{a_Q}^2 \leq C \left(\|p^0\|_{a_Q}^2 + \int_0^T \|f\|_{[L^2(\Omega)]^2}^2 dt \right) \quad (94)$$

Similarly, by taking $v = \frac{\partial p_{\text{ms}}}{\partial t}$ in (15) and integrating over $(0, T)$, we obtain

$$\frac{1}{2} \int_0^T \left\| \frac{\partial p_{\text{ms}}}{\partial t} \right\|_c^2 dt + \frac{1}{2} \|p_{\text{ms}}(T, \cdot)\|_{a_Q}^2 \leq C \left(\|p^0\|_{a_Q}^2 + \int_0^T \|f\|_{[L^2(\Omega)]^2}^2 dt \right) \quad (95)$$

At the same time, by (2), we can see that

$$\mathcal{A}p = f - \mathcal{C} \frac{\partial p}{\partial t}. \quad (96)$$

Thus, we have

$$\|\mathcal{A}p\|_{[L^2(\Omega)]^2}^2 \leq C \left(\|f\|_{[L^2(\Omega)]^2}^2 + \left\| \frac{\partial p}{\partial t} \right\|_c \right) \quad (97)$$

By the definition of p and p_{ms} in (2) and (15), respectively, we can get that $\forall v \in V_{\text{ms}}$ and $t \in (0, T)$, we have

$$c \left(\frac{\partial(p - p_{\text{ms}})}{\partial t}, v \right) + a_Q(p - p_{\text{ms}}, v) = 0. \quad (98)$$

Thus, we have

$$\begin{aligned} & \frac{1}{2} \frac{d}{dt} \|p - p_{\text{ms}}\|_c^2 + \|p - p_{\text{ms}}\|_{a_Q}^2 \\ &= c \left(\frac{\partial(p - p_{\text{ms}})}{\partial t}, p - p_{\text{ms}} \right) + a_Q(p - p_{\text{ms}}, p - p_{\text{ms}}) \\ &= c \left(\frac{\partial(p - p_{\text{ms}})}{\partial t}, p - R_{\text{ms}}p \right) + a_Q(p - p_{\text{ms}}, p - R_{\text{ms}}p) \\ &\leq \left\| \frac{\partial(p - p_{\text{ms}})}{\partial t} \right\|_c \|p - R_{\text{ms}}p\|_c + \|p - p_{\text{ms}}\|_{a_Q} \|p - R_{\text{ms}}p\|_{a_Q} \\ &\leq \left(\left\| \frac{\partial p}{\partial t} \right\|_c + \left\| \frac{\partial p_{\text{ms}}}{\partial t} \right\|_c \right) \|p - R_{\text{ms}}p\|_c + \frac{1}{2} \|p - p_{\text{ms}}\|_{a_Q}^2 + \frac{1}{2} \|p - R_{\text{ms}}p\|_{a_Q}^2. \end{aligned} \quad (99)$$

Integrating over $(0, T)$ and using (96) by Lemma 4 with (18), we obtain

$$\begin{aligned}
& \frac{1}{2} \|p(T, \cdot) - p_{\text{ms}}(T, \cdot)\|_c^2 + \frac{1}{2} \int_0^T \|p - p_{\text{ms}}\|_{a_Q}^2 dt \\
& \leq \int_0^T \left(\left\| \frac{\partial p}{\partial t} \right\|_c + \left\| \frac{\partial p_{\text{ms}}}{\partial t} \right\|_c \right) \|p - R_{\text{ms}}p\|_c dt + \frac{1}{2} \int_0^T \|p - R_{\text{ms}}p\|_{a_Q}^2 dt \\
& \leq \left(\int_0^T \left(\left\| \frac{\partial p}{\partial t} \right\|_c + \left\| \frac{\partial p_{\text{ms}}}{\partial t} \right\|_c \right)^2 dt \right)^{\frac{1}{2}} \left(\int_0^T \|p - R_{\text{ms}}p\|_c^2 dt \right)^{\frac{1}{2}} + \frac{1}{2} \int_0^T \|p - R_{\text{ms}}p\|_{a_Q}^2 dt \\
& \leq \left(\int_0^T \left(\left\| \frac{\partial p}{\partial t} \right\|_c + \left\| \frac{\partial p_{\text{ms}}}{\partial t} \right\|_c \right)^2 dt \right)^{\frac{1}{2}} \left(\int_0^T CH^4 \underline{\kappa}^{-2} \left(\|f\|_{[L^2(\Omega)]^2} + \left\| \frac{\partial p}{\partial t} \right\|_c \right)^2 dt \right)^{\frac{1}{2}} \\
& \quad + \int_0^T CH^2 \underline{\kappa}^{-1} \left(\|f\|_{[L^2(\Omega)]^2} + \left\| \frac{\partial p}{\partial t} \right\|_c \right)^2 dt \\
& \leq CH^2 \underline{\kappa}^{-1} \int_0^T \left(\left\| \frac{\partial p}{\partial t} \right\|_c^2 + \left\| \frac{\partial p_{\text{ms}}}{\partial t} \right\|_c^2 + \|f\|_{[L^2(\Omega)]^2}^2 \right) dt.
\end{aligned} \tag{100}$$

Combining (94), (95) and (100), we get the result in the theorem. \square

5 Numerical Examples

In this section, we present two numerical examples with high-contrast media to verify the convergence of our proposed method, using a fine-scale approximation p_f as a reference solution. We will compute the coarse cell average \bar{p}_f of the fine-scale solution p_f and \bar{p}_{ms} of the multiscale solution p_{ms} , and compare the relative L_2 error of coarse cell average, i.e.

$$e_{L_2}^{(i)} = \|\bar{p}_{f,i} - \bar{p}_{\text{ms},i}\|_{L^2}, \quad \|\bar{p}_{f,i} - \bar{p}_{\text{ms},i}\|_{L_2}^2 = \frac{\sum_K (\bar{p}_{f,i}^K - \bar{p}_{\text{ms},i}^K)^2}{\sum_K (\bar{p}_f^K)^2}, \quad \bar{p}_{f,i}^K = \frac{1}{|K|} \int_K p_{f,i} dx. \tag{101}$$

In all the experiments, we take the spatial domain to be $\Omega = (0, 1)^2$ and the fine mesh size to be $h = 1/256$. An example of the media κ_1 and κ_2 used in the experiments is illustrated in Figure 3. In the figure, the contrast values, i.e. the ratio of the maximum and the minimum in Ω , of the media are $\bar{\kappa}_1 = \bar{\kappa}_2 = 10^4$. Unless otherwise specified, we set $\sigma = 1$.

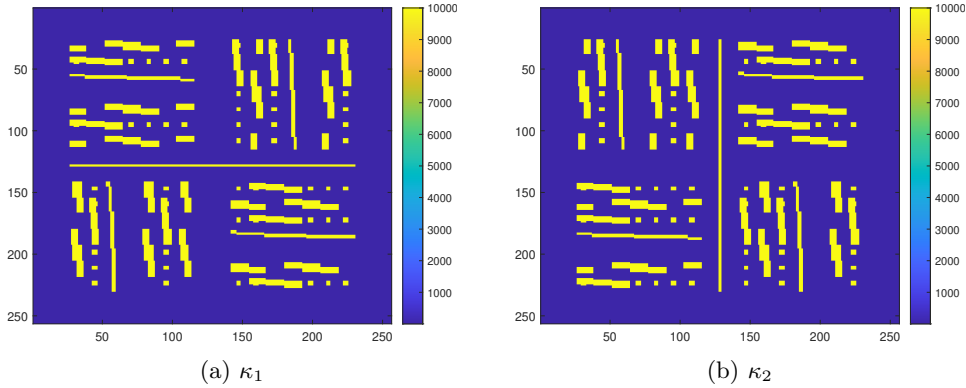


Figure 3: High contrast permeability field

5.1 Experiment 1 static case

In this experiment, we consider the dual continuum model under steady state

$$\begin{aligned} -\operatorname{div}(\kappa_1 \nabla p_1) + \sigma(p_1 - p_2) &= f_1, \\ -\operatorname{div}(\kappa_2 \nabla p_2) - \sigma(p_1 - p_2) &= f_2. \end{aligned} \tag{102}$$

The source terms are given as $f_1(x, y) = 1$ and $f_2(x, y)$ as shown in Figure 4. In Figure 5, we plot the fine-scale solution, the coarse-scale average and the NLMC coarse-scale solution with coarse mesh size $H = 1/64$ and number of oversampling layers $m = 8$, from which we observe very good agreement between the coarse-scale average and the NLMC solution. In Table 1, we present the relative L^2 error with varying coarse grid size. With the number of oversampling layers satisfying the sufficient condition, we can see that the error converges. We also compare the performance of different numbers of oversampling layers under fixed coarse mesh size H . The results are summarized in Table 2 for $H = 1/32$ and Table 3 for $H = 1/64$. It can be seen that the error decays quickly with respect to the number of oversampling layers m for both cases, which verifies the fact that the oversampling region has to be sufficiently large to obtain quality numerical approximations.

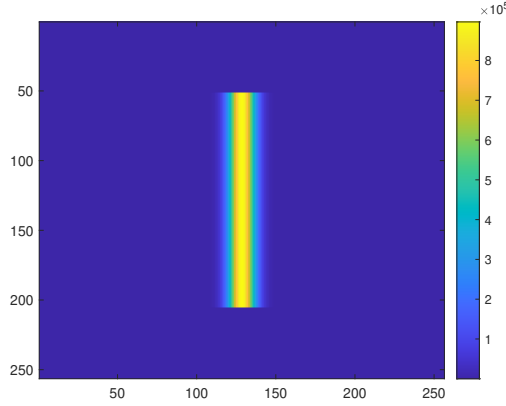


Figure 4: Source term f_2 in Experiment 1.

H	m	$e_{L^2}^{(1)}$	$e_{L^2}^{(2)}$
1/8	3	96.7318%	88.9818%
1/16	5	32.3229%	19.3473%
1/32	6	0.6045%	0.3680%
1/64	8	0.0550%	0.0296%

Table 1: Convergence of e_{L_2} with respect to coarse mesh size H in Experiment 1.

5.2 Experiment 2: time-dependent case

The time dependent case faces the similar issue with the error. $f_1(x, y) = 1$ and $f_2(x, y)$ is depicted in Figure 6, which represents a simplified five-spot well rate. The temporal domain is $[0, T]$ with final time $T = 5$. In Figure 7, we plot the fine-scale solution, the coarse-scale average and the NLMC coarse-scale solution with coarse mesh size $H = 1/64$ and number of oversampling layers $m = 8$. Again, the NLMC solution is a good approximation for the coarse-scale average. In Figure 8, we depict the change of pressure at different time steps. In Table 4, we present the

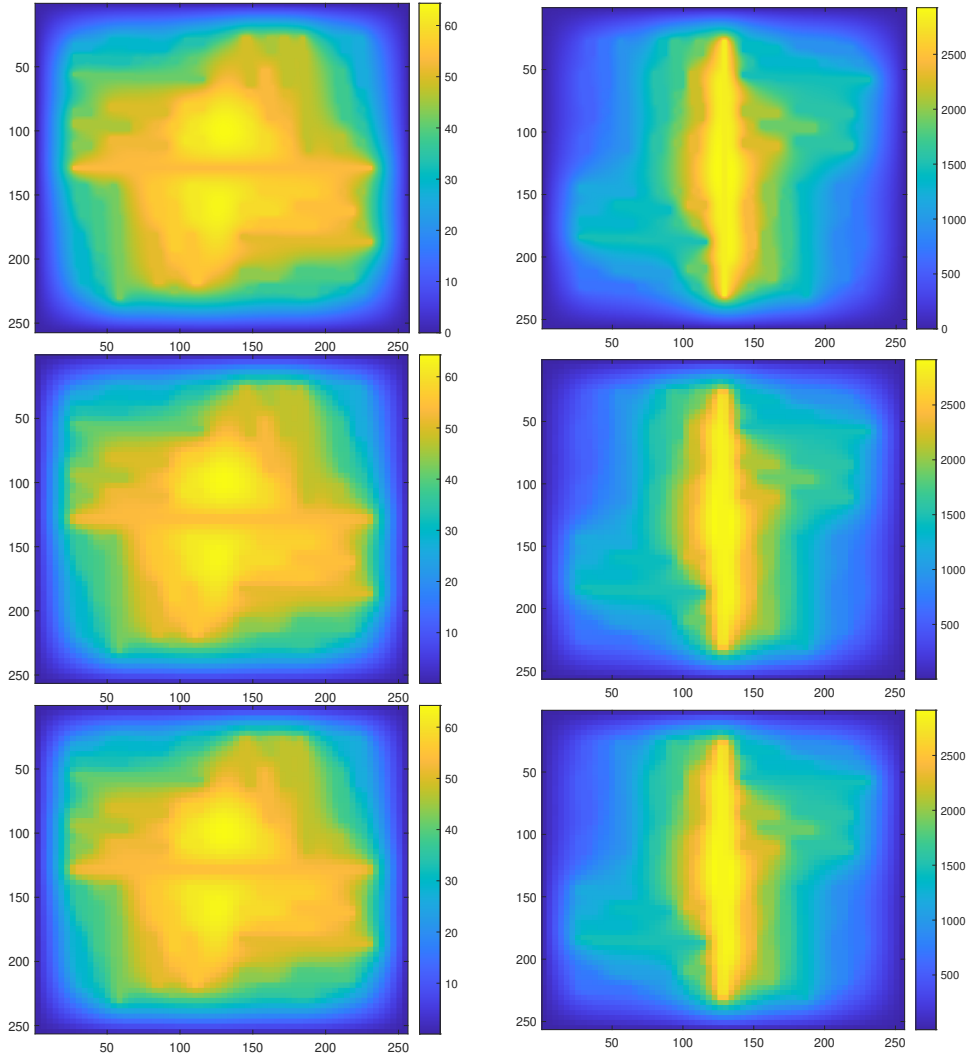


Figure 5: Plots of the numerical approximations of pressure with coarse mesh size $H = 1/64$ and $m = 8$ oversampling layers in Experiment 1. Left: first continuum. Right: second continuum. First row: fine-scale solution. Second row: coarse-scale average of fine-scale solution. Third row: NLMC solution.

m	Area Ratio	$e_{L^2}^{(1)}$	$e_{L^2}^{(2)}$
3	4.79%	99.3677%	93.9357%
4	7.91%	76.6083%	55.1631%
5	11.81%	8.6605%	5.3115%
6	16.50%	0.6045%	0.3680%

Table 2: Comparison of e_{L^2} error with different number of oversampling layers m for $H = 1/32$ in Experiment 1.

relative L^2 error with varying coarse grid size. Again, with the number of oversampling layers satisfying the sufficient condition, we can see that the error converges very well.

m	Area Ratio	$e_{L_2}^{(1)}$	$e_{L_2}^{(2)}$
2	0.61%	99.9102%	97.9631%
4	1.98%	99.1268%	91.9240%
6	4.13%	11.8898%	6.3181%
7	5.49%	0.7959%	0.4219%
8	7.06%	0.0550%	0.0296%

Table 3: Comparison of e_{L_2} error with different number of oversampling layers m for $H = 1/64$ in Experiment 1.

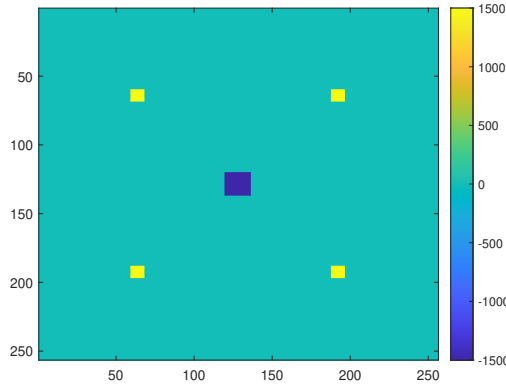


Figure 6: Source term f_2 in Experiment 2.

H	m	$e_{L_2}^{(1)}$	$e_{L_2}^{(2)}$
1/8	3	20.6422%	58.4975%
1/16	5	1.1245%	2.6226%
1/32	6	0.0254%	0.0717%
1/64	8	0.0017%	0.0037%

Table 4: Convergence of e_{L_2} with respect to coarse mesh size H in Experiment 2.

6 Conclusions

In this paper, we investigated the non-local multicontinuum (NLMC) upscaling method for a dual continuum model in fractured porous media. Localized multiscale basis functions that separate each continuum are constructed. To find the basis, we solve local problems subject to energy minimization constraints in oversampling coarse regions. It is shown that the basis functions equip the method with coarse mesh convergence. Some numerical examples are presented to support the theory. The numerical examples also indicate that the proposed method provides accurate and efficient coarse-grid approximation.

References

- [1] A. Abdulle. On a priori error analysis of fully discrete heterogeneous multiscale fem. *SIAM J. Multiscale Modeling and Simulation*, 4(2):447–459, 2005.
- [2] Todd Arbogast, Jim Douglas, Jr, and Ulrich Hornung. Derivation of the double porosity model of single phase flow via homogenization theory. *SIAM Journal on Mathematical Analysis*, 21(4):823–836, 1990.

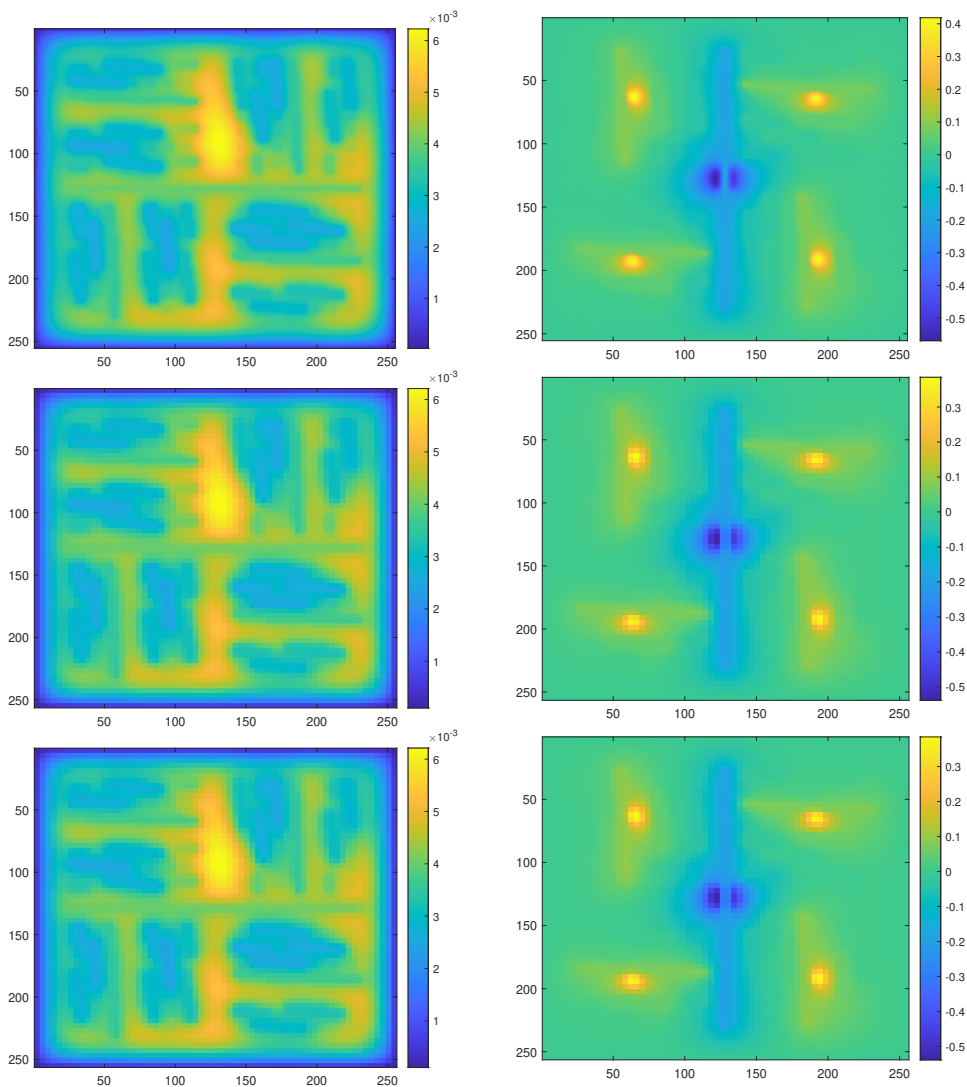


Figure 7: Plots of the numerical approximations of final-time pressure with coarse mesh size $H = 1/64$ and $m = 8$ oversampling layers in Experiment 2. Left: first continuum. Right: second continuum. First row: fine-scale solution. Second row: coarse-scale average of fine-scale solution. Third row: NLMC solution.

- [3] GI Barenblatt, Iu P Zheltov, and IN Kochina. Basic concepts in the theory of seepage of homogeneous liquids in fissured rocks [strata]. *Journal of applied mathematics and mechanics*, 24(5):1286–1303, 1960.
- [4] Victor Calo, Yalchin Efendiev, and Juan Galvis. A note on variational multiscale methods for high-contrast heterogeneous porous media flows with rough source terms. *Advances in water resources*, 34(9):1177–1185, 2011.
- [5] Siu Wun Cheung, Eric T. Chung, Yalchin Efendiev, and Wing Tat Leung. Explicit and energy-conserving constraint energy minimizing generalized multiscale discontinuous galerkin method for wave propagation in heterogeneous media. *arXiv preprint, arXiv:2009.00991*, 2020.

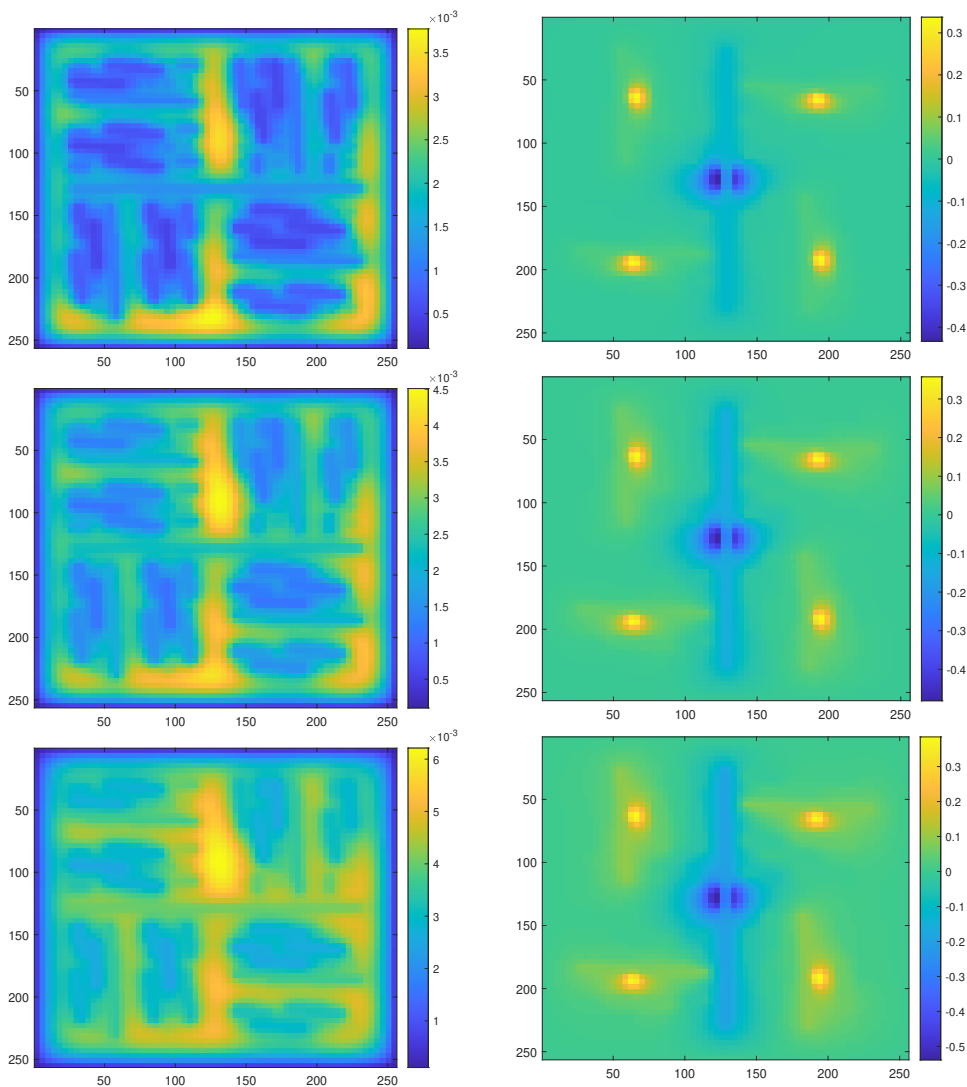


Figure 8: Plots of the NLMC numerical approximations of pressure at various time instants with coarse mesh size $H = 1/64$ and $m = 8$ oversampling layers in Experiment 2. Left: first continuum. Right: second continuum. First row: $t = 1.25$. Second row: $t = 2.5$. Third row: $t = 5$.

- [6] Siu Wun Cheung, Eric T Chung, Yalchin Efendiev, Wing Tat Leung, and Maria Vasilyeva. Constraint energy minimizing generalized multiscale finite element method for dual continuum model. *Communications in Mathematical Sciences*, 18:663–685, 2020.
- [7] Siu Wun Cheung, Eric T Chung, and Wing Tat Leung. Constraint energy minimizing generalized multiscale discontinuous galerkin method. *Journal of Computational & Applied Mathematics*, 380:112960, 2020.
- [8] Eric Chung, Yalchin Efendiev, and Thomas Y Hou. Adaptive multiscale model reduction with generalized multiscale finite element methods. *Journal of Computational Physics*, 320:69–95, 2016.

- [9] Eric Chung, Yalchin Efendiev, and Wing Tat Leung. Constraint energy minimizing generalized multiscale finite element method in the mixed formulation. *Computational Geosciences*, 22(3):677–693, 2018.
- [10] Eric T Chung, Yalchin Efendiev, Tat Leung, and Maria Vasilyeva. Coupling of multiscale and multi-continuum approaches. *GEM-International Journal on Geomathematics*, 8(1):9–41, 2017.
- [11] Eric T Chung, Yalchin Efendiev, and Wing Tat Leung. Constraint energy minimizing generalized multiscale finite element method. *Computer Methods in Applied Mechanics and Engineering*, 339:298–319, 2018.
- [12] Eric T. Chung, Yalchin Efendiev, Wing Tat Leung, Yating Wang, and Maria Vasilyeva. Non-local multi-continua upscaling for flows in heterogeneous fractured media. *Journal of Computational Physics*, 372:22–34, 2018.
- [13] ET Chung, Y Efendiev, and G Li. An adaptive GMSFEM for high-contrast flow problems. *Journal of Computational Physics*, 273:54–76, 2014.
- [14] Jim Douglas Jr and T Arbogast. Dual porosity models for flow in naturally fractured reservoirs. *Dynamics of Fluids in Hierarchical Porous Media*, pages 177–221, 1990.
- [15] L.J. Durlofsky. Numerical calculation of equivalent grid block permeability tensors for heterogeneous porous media. *Water Resour. Res.*, 27:699–708, 1991.
- [16] W. E and B. Engquist. Heterogeneous multiscale methods. *Comm. Math. Sci.*, 1(1):87–132, 2003.
- [17] W. E, P. Ming, and P. Zhang. Analysis of the heterogeneous multiscale method for elliptic homogenization problems. *J. Amer. Math. Soc.*, 18(1):121–156, 2005.
- [18] Y. Efendiev, J. Galvis, and T. Hou. Generalized multiscale finite element methods. *Journal of Computational Physics*, 251:116–135, 2013.
- [19] Y. Efendiev, J. Galvis, and X.H. Wu. Multiscale finite element methods for high-contrast problems using local spectral basis functions. *Journal of Computational Physics*, 230:937–955, 2011.
- [20] Y. Efendiev, T. Hou, and X.H. Wu. Convergence of a nonconforming multiscale finite element method. *SIAM J. Numer. Anal.*, 37:888–910, 2000.
- [21] Yalchin Efendiev, Eduardo Gildin, and Yanfang Yang. Online adaptive local-global model reduction for flows in heterogeneous porous media. *Computation*, 4(2):22, 2016.
- [22] TT Garipov, M Karimi-Fard, and HA Tchelepi. Discrete fracture model for coupled flow and geomechanics. *Computational Geosciences*, 20(1):149–160, 2016.
- [23] T. Hou and X.H. Wu. A multiscale finite element method for elliptic problems in composite materials and porous media. *J. Comput. Phys.*, 134:169–189, 1997.
- [24] T.J.R. Hughes, G.R. Feijóo, L. Mazzei, and J.-B. Quinicy. The variational multiscale method - a paradigm for computational mechanics. *Comput. Methods Appl. Mech. Engrg.*, 127:3–24, 1998.
- [25] TJR Hughes and G Sangalli. Variational multiscale analysis: the fine-scale Green’s function, projection, optimization, localization, and stabilized methods. *SIAM Journal on Numerical Analysis*, 45(2):539–557, 2007.

- [26] O. Iliev, R. Lazarov, and J. Willems. Variational multiscale finite element method for flows in highly porous media. *Multiscale Model. Simul.*, 9(4):1350–1372, 2011.
- [27] M Karimi-Fard, LJ Durlofsky, and K Aziz. An efficient discrete-fracture model applicable for general-purpose reservoir simulators. *SPE-88812-PA*, 2004.
- [28] M Karimi-Fard and A Firoozabadi. Numerical simulation of water injection in 2d fractured media using discrete-fracture model. *SPE-71615-MS*, 2001.
- [29] H Kazemi, LS Merrill Jr, KL Porterfield, PR Zeman, et al. Numerical simulation of water-oil flow in naturally fractured reservoirs. *Society of Petroleum Engineers Journal*, 16(06):317–326, 1976.
- [30] Jun Sur Richard Park, Siu Wun Cheung, and Tina Mai. Multiscale simulations for multi-continuum richards equations. *arXiv preprint, arXiv:2010.09181*, 2020.
- [31] Jun Sur Richard Park, Siu Wun Cheung, Tina Mai, and Viet Ha Hoang. Multiscale simulations for upscaled multi-continuum flows. *Journal of Computational & Applied Mathematics*, 374:112782, 2020.
- [32] K Pruess and TN Narasimhan. On fluid reserves and the production of superheated steam from fractured, vapor-dominated geothermal reservoirs. *Journal of Geophysical Research: Solid Earth*, 87(B11):9329–9339, 1982.
- [33] Maria Vasilyeva, Eric T Chung, Siu Wun Cheung, Yating Wang, and Georgy Prokopev. Nonlocal multicontinua upscaling for multicontinua flow problems in fractured porous media. *Journal of Computational & Applied Mathematics*, 355:258–267, 2019.
- [34] Maria Vasilyeva, Eric T. Chung, Wing Tat Leung, and Valentin Alekseev. Nonlocal multi-continuum (nlmc) upscaling of mixed dimensional coupled flow problem for embedded and discrete fracture models. *GEM International Journal on Geomathematics*, 10:23, 2019.
- [35] Min Wang, Siu Wun Cheung, Eric T. Chung, Maria Vasilyeva, and Yuhe Wang. Generalized multiscale multicontinuum model for fractured vuggy carbonate reservoirs. *Journal of Computational and Applied Mathematics*, 366:112370, 2020.
- [36] JE Warren, P Jj Root, et al. The behavior of naturally fractured reservoirs. *Society of Petroleum Engineers Journal*, 3(03):245–255, 1963.
- [37] X.H. Wu, Y. Efendiev, and T.Y. Hou. Analysis of upscaling absolute permeability. *Discrete and Continuous Dynamical Systems, Series B.*, 2:158–204, 2002.
- [38] Yu-Shu Wu, Karsten Pruess, et al. A multiple-porosity method for simulation of naturally fractured petroleum reservoirs. *SPE Reservoir Engineering*, 3(01):327–336, 1988.
- [39] Lina Zhao and Eric Chung. An analysis of the nlmc upscaling method for high contrast problems. *Journal of Computational and Applied Mathematics*, 367:112480, 2020.